Tomographic Reconstruction Methods for Decomposing Directional Components

Kongskov, Rasmus Dalgas; Dong, Yiqiu

Publication date:
2017

Document Version
Publisher's PDF, also known as Version of record

Tomographic Reconstruction Methods for Decomposing Directional Components

Rasmus Dalgas Kongskov* Yiqiu Dong*

August 30, 2017

Abstract

X-ray computed tomography technique has many different practical applications. In this paper, we propose two new reconstruction methods that can decompose objects at the same time. By incorporating direction information, the proposed methods can decompose objects into various directional components. Furthermore we propose a method to obtain the direction information in the objects directly from the measured sinogram data. We demonstrate the proposed methods on simulated and real samples to show their practical applicability. The numerical results show the differences between the two methods and effectiveness as dealing with fibre-crack decomposition problem.

1 Introduction

X-ray computed tomography (CT) is a highly used non-invasive imaging technique. Applications of this technique ranges from biological and chemical science, to structural and material science, where the resolution also varies from large scale (meters) to micro-scale (nano-meters). In CT technique, reconstruction methods play a fundamental role, and very often after reconstruction we need segment or decompose the objects into different components. In this paper, we focus on directional objects, whose textures are mainly along one direction. One important example of directional objects is fibres, such as optical fibres, glass fibres, carbon fibres, etc. When analyzing fibre materials, CT scanners can be used to investigate interior properties, for example irregularities, see [21, 23, 12]. A specific irregularity that is often sought for in fibre materials are cracks. Both the fibres and the cracks can be regarded as directional components. Based on this application, we will propose new methods for reconstructing and decomposing directional components simutaneously.

The CT technique is based on the X-ray attenuations as X-rays pass through objects. According to Lambert-Beers law, the measured data, i.e. the sinogram, can be considered as line integrals on the attenuation coefficients of the object [5]. In the continuous setting, we call this integral as Radon transform, and in the discrete setting we can write it as a linear equation:

$$A\mathbf{z} \approx \mathbf{b}, \tag{1}$$

*Department of Applied Mathematics and Computer Science, Technical University of Denmark, 2800 Kgs. Lyngby, Denmark (rara@dtu.dk, yido@dtu.dk.

where $A \in \mathbb{R}^{N\times M^2}$ represents the CT process, $\mathbf{z} \in \mathbb{R}^{M^2}$ represents the object to be reconstruct, and $\mathbf{b} \in \mathbb{R}^N$ denotes measured noisy data. The data is measured with N_ϕ scanning angles and N_t detector bins, wihch gives $N = N_\phi N_t$. For simplicity we consider 2D parallel beam geometry, the work introduced in the paper can be easily extended to fan beam geometry. In addition, we assume that the scanning angles are fully around the objects.

The most widely used reconstruction method for CT isFiltered Back-Projection (FBP) [20], which is based on the analytical formulation of inverse Radon transform. Therefore, FBP implicitly assumes to have continuously measured data from the whole 180° angular range. FBP is very efficient, and with sufficient measurements low noise level the method provides good results. But when we deal with noisy data and underdetermined system, FBP will introduce many artifacts. In order to overcome the drawback from FBP and be able to deal with noisy and/or limited data, variational methods have been used for many inverse problems including CT reconstruction, see [1, 24] for more details. In this paper, we assume that the sinogram data are corrupted by additive white Gaussian noise, which ends up with the following variational model

$$\min_{\mathbf{z}} \ \frac{1}{2}\|A\mathbf{z} - \mathbf{b}\|_2^2 + \mathcal{R}(\mathbf{z}). \tag{2}$$

In (2) $\mathcal{R}(\mathbf{z})$ is called as regularization term, which incorporates the prior information on the objects. Many regularization techniques have been proposed, and one of the most commonly used for imaging problems is total variation (TV). TV was first introduced in [22] for image restoration and afterwards was used for CT reconstruction in e.g. [8, 25].

In order to decompose the objects into several components, image decomposition methods was first proposed in [6] by using infimal convolution. The idea is to define two convex functionals J_1 and J_2 with respect to two components z_1 and z_2 according to their properties, respectively, then by solving the optimization problem

$$\inf\{J_1(z_1) + J_2(z_2)\} \quad \text{s.t.} \quad z = z_1 + z_2$$

to obtain decomposition results. Based on different applications, many image decomposition methods were proposed, e.g. [17, 9, 26, 2, 3, 10, 11]. Recently, this technique is also applied to CT problems to decompose the reconstruction into the object component, limited data artifacts and noise component [16].

In this paper, we propose two methods to decompose the objects into directional components. One method is motivated from the microlocal analysis results in [19], and decomposes the objects by splitting the sinogram directly. In order to suppress artifacts from limited data, variational methods with proper regularizations are introduced. The other method is based on image decomposition by using the infimal convolution. We compare the two methods by discussing their theoretical differences, and also demonstrate their performance through empirical examples. In addition, to define the directional components, we also introduce a method to estimate the main direction of an object directly from its sinogram.

The paper is organized as follows. In section 2 we review a regularization technique proposed in [14] for incorporating direction information. Furthermore, we propose a method to estimate the main direction of an object directly from its sinogram data. In section 3 we introduce the sinogram splitting method, where by

splitting the sinogram we are able to obtain components along different directions. In section 4 a image decomposition method by using directional regularization is proposed to decompose directional components. Numerical experiments are carried out in section 5, and in section 6 conclusions are drawn.

2 Directional regularization in CT reconstruction

We start this section by reviewing a directional regularization, called as directional total variation (DTV), proposed in [4, 14, 13]. This regularization is one kind of anisotropic TV, and very effective for reconstructing directional objects, whose textures are mainly along one specific direction. Afterwards taking CT scanning geometry into account we propose a method to estimate the main direction of objects directly from the sinogram data.

2.1 Directional regularization

In order to incoporate direction information, a directional regularization, called as directional total variation (DTV), was introduced for image denoising and deblurring in [4, 14, 13]. DTV builds on the prior that the object is piece-wise constant and its textures are along one main direction. For an image $\mathbf{z} \in \mathbb{R}^{M\times M}$, its DTV can be defined as

$$\mathrm{DTV}_{\theta,a}(\mathbf{z}) = \sum_{i,j} |R_\theta \Lambda_a (\nabla \mathbf{z})_{i,j}|_2,$$

where

$$R_\theta = \begin{pmatrix} \cos\theta & -\sin\theta \\ \cos\theta & \sin\theta \end{pmatrix} \quad \text{and} \quad \Lambda_a = \begin{pmatrix} 1 & 0 \\ 0 & a \end{pmatrix}, \tag{3}$$

denote the rotation matrix with the angle $\theta \in (0, 2\pi]$ and the scaling matrix with the paramter $a \in (0, 1]$, respectively. In addition, the gradient operator $\nabla : \mathbb{R}^{M\times M} \to \mathbb{R}^{2M\times M}$ is defined as

$$\nabla \mathbf{z} = \begin{pmatrix} \nabla_{x_1}\mathbf{z} \\ \nabla_{x_2}\mathbf{z} \end{pmatrix} \quad \text{and} \quad (\nabla \mathbf{z})_{i,j} = \begin{pmatrix} (\nabla_{x_1}\mathbf{z})_{i,j} \\ (\nabla_{x_2}\mathbf{z})_{i,j} \end{pmatrix}$$

where ∇_{x_1} and ∇_{x_2} denote the derivatives along the two dimensions x_1 and x_2, respectively, and can be obtained by applying a forward finite difference scheme with symmetric boundary condition, i.e.,

$$(\nabla_{x_1}\mathbf{z})_{i,j} = \begin{cases} z_{i+1,j} - z_{i,j}, & \text{if } i < M, \\ 0, & \text{if } i = M, \end{cases} \quad \text{and } (\nabla_{x_2}\mathbf{z})_{i,j} = \begin{cases} z_{i,j+1} - z_{i,j}, & \text{if } j < M, \\ 0, & \text{if } j = M. \end{cases}$$

In Figure 1, we give an example to illustrate how the DTV regularization performs when reconstructing directional objects from CT data. In this example, the underdetermined rate, i.e., $\frac{N}{M^2}$, equals $\frac{2}{3}$, and the data are corrupted by 1% additive white Gaussian noise. We compare the result by using the DTV regularization in eqn:varprop with the one from FBP and the one by using total variation (TV) as regularization. It is obvious that the DTV result is superior both quantitatively (based on the peak signal-to-noise ratio, psnr in short, measure) and visually.

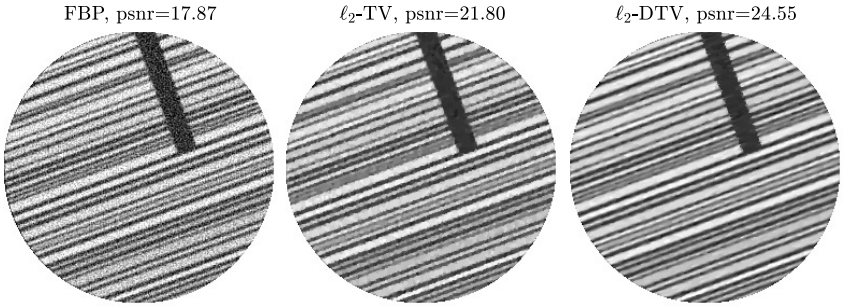

Figure 1: Comparison on simulated CT reconstruction problem. Regularization parameters for the ℓ_2-TV and ℓ_2-DTV methods are tuned to maximize the peak-signal-to-noise ratio (psnr). The parameters in DTV are chosen as $a = 0.15$ and $\theta = 20°$.

2.2 Direction estimation from sinogram data

In order to use DTV as regularization we have to select the parameters a and θ. Based on the results in [14] with a good direction estimation $a = 0.15$ usually provides good results. In this section, we focus on the main direction estimation, and propose a method to estimate it directly from sinogram data.

In [13] a direction estimator based on Fourier transform was proposed. This estimator is according to the fact that 2D Fourier basis functions can be seen as images with a significant main direction. Therefore, if the textures of the image are mainly along one direction, the magnitude of the coefficients corresponding to the Fourier basis along the same direction will be relatively large. Although this estimator is robust with respect to the noise, it requries the information in image domain. But in CT reconstruction, we only have sinogram data. To avoid estimating the main direction θ from the reconstruction, we introduce a new direction estimator based on CT scanning geometry.

Since CT scan is around the objects, the measurements are strongly related with the scanning angle. If we consider the case that the scanning angle is relatively close to the main direction θ, then the projections will be through the objects or through the gaps among the objects. Hence, the measurements along θ will be oscillating. Then, we can utilize 1D Fourier transform to check if the measurements along each scanning angle are oscillating, and the largest magnitude of the Fourier coefficients should correspond to the main direction. The detailed algorithm for estimating the main direction is given in algorithm 1. Note that this direction estimator is not limited to parallel-beam tomography, since a similar oscillating signal also appears when the fan-beam geometry is used.

In order to show the performance of our direction estimator, we test it on a simulated phantom and a real object from [12]. In both cases we simulate the projections and the noise. In Table 1 we list the estimated direction under different level of additive Gaussian noise, ρ, and in Figure 2 we show the two objects with their sinograms. Furthermore, we indicate the estimated direction from the noise-free sinogram and the sum of the magnitudes along each angle from algorithm 1. Based on these empirical tests it is clear that up to 20% Gaussian noise the new direction estimator is robust with respect to the noise.

Algorithm 1 Main Direction Estimator

1: Input the sinoogram data b and the measurement angles $\{\phi_m\}$.

2: Compute 1D Fourier transform along each angle ϕ_m:

$$\hat{b}_{\omega,m} = \sum_{l=0}^{N_t-1} b_{l,m} \mathrm{e}^{-\frac{2\pi\iota\omega l}{N_t}}.$$

3: Calculate the sum of the magnitudes along each angle ϕ_m and find its maximizer:

$$h = \underset{m}{\operatorname{argmax}} \sum_{\omega} |\hat{b}_{\omega,m}|.$$

4: Return the main direction $\theta = \phi_h$.

ρ (%)	0	1	3	5	10	20	30	40
Phantom	20.1	20.1	20.1	20.1	20.1	20.1	20.1	31.7
Real	81.5	81.7	81.5	80.9	81.7	79.5	-1.1	-34.9

Table 1: Direction estimation results for the phantom and real objects shown in fig. 2. Note that the exact main directino for the phantom is 20°.

3 Sinogram Splitting Method

Microlocal analysis (MLA) have been used to determine which singular features such as edges we can expect to recover in a range of continuous tomography problems. In [19] the relation between singularities in a function f and singularities in its Radon transform $\mathcal{A}f$ is described. The paradigm that is described in [19] is further outlined in [15] as follows:

$\mathcal{A}$ detects singularities of f perpendicular to the line of integration ("visible" singularities), but singularities of f in other ("invisible") directions do not create singularities of $\mathcal{A}f$ near the line of integration.

The fact that singularities only propagate when X-rays are perpendicular to them inspired us to split the sinogram in order to decompose the objects into several components along different directions. Here, each splitted part of the sinogram is related to an object component where the directions of the singularities, in the object-domain, are limited. In the following, we focus on a two-component split, which can be easily extended to decompose any integer amount of components with different directions.

Assume the two object components are $\mathbf{u}$ and $\mathbf{w}$, and both are in $\mathbb{R}^{M^2}$. The textures of $\mathbf{u}$ are mainly along the directions with the angles $\phi_u \in \mathbb{R}^K$, and $\mathbf{w}$ mainly contains the textures along the other angles $\phi_w \in \mathbb{R}^{N-K}$. Based on MLA, in order to reconstruct the textures in certain angles, we need the measurements along the same angles. Then, we split the sinogram and the system matrix according to ϕ_u and ϕ_w and obtain:

$$A_u\mathbf{u} \approx \mathbf{b}_u \qquad \text{and} \qquad A_w\mathbf{w} \approx \mathbf{b}_w, \tag{4}$$

where $A_u \in \mathbb{R}^{KN_t \times M^2}$ and $A_w \in \mathbb{R}^{(N-K)N_t \times M^2}$ are the splitted matrices, and $\mathbf{b}_u \in \mathbb{R}^{KN_t}$ and $\mathbf{b}_w \in \mathbb{R}^{(N-K)N_t}$ are the splitted noisy sinograms. Here, we

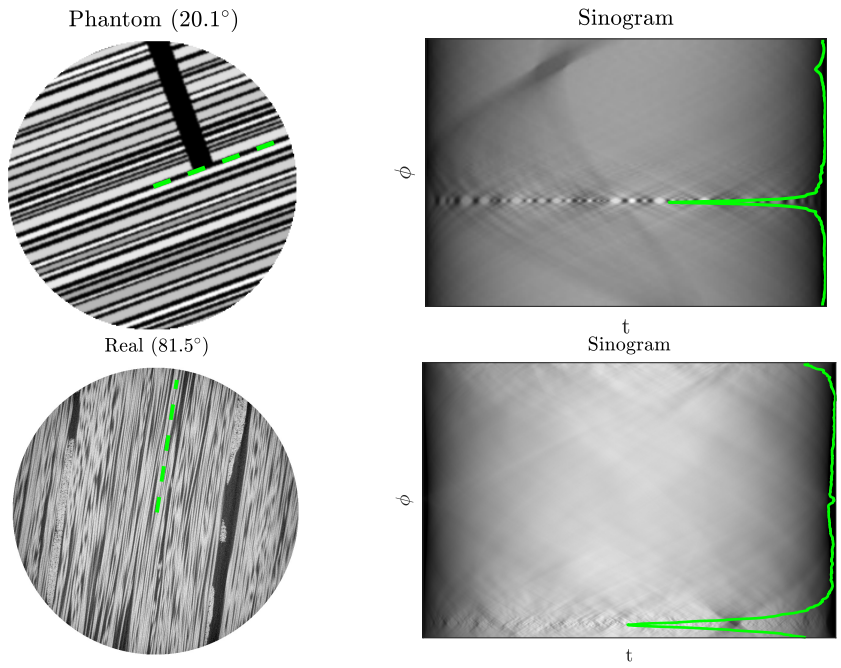

Figure 2: Left: the objects with estimated direction from the noise-free sinogram. Right: the noise-free sinogram overlayed with the plot of the sum of the magnitudes.

assume that K is a natural number and larger than 1 in order to avoid reconstructing $\mathbf{u}$ from only one angle measurements.

To solve the linear systems in (4), we can use FBP. Since FBP is based on the analytical solution of the Radon transform in continuous setting, it requires to scan the objects from all angles and to have enough projections for each angle. With limited angle problems, the data according to the missing angles are implicitly filled by 0. For the systems (4) it is identical to the assumptions:

$$A_u \mathbf{w} = 0, \quad \text{and} \quad A_w \mathbf{u} = 0. \tag{5}$$

On one hand, due to the artificial singularities in the sinograms at the transition between the measured data and the assumed 0-data, artifacts will appear in both $\mathbf{u}$ and $\mathbf{w}$; on the other hand, according to the assumptions we have

$$\begin{bmatrix} A_u \\ A_w \end{bmatrix} (\mathbf{u} + \mathbf{w}) \approx \begin{bmatrix} \mathbf{b}_u \\ \mathbf{b}_w \end{bmatrix}, \tag{6}$$

which means that $\mathbf{u}+\mathbf{w}$ is reconstructed from the whole sinogram, and the limited angle artifacts in $\mathbf{u}$ and $\mathbf{w}$ will be cancelled.

Besides the limited angle artifacts appearing in reconstruction results from FBP, FBP is also very sensitive to the noise in the sinogram. In order to obtain good reconstructions from noisy data with limited angles, we can use variational methods by incorporating prior information on the individual components. Based

on the linear systems (4) we get the following two variational models for reconstructing $\mathbf{u}$ and $\mathbf{w}$:

$$\min_{\mathbf{u}\geq 0} \|A_u\mathbf{u} - \mathbf{b}_u\|_2 + \mathcal{R}_u(\mathbf{u}), \tag{7}$$

$$\min_{\mathbf{w}\geq 0} \|A_w\mathbf{w} - \mathbf{b}_w\|_2 + \mathcal{R}_w(\mathbf{w}), \tag{8}$$

where the regularization terms $\mathcal{R}_u$ and $\mathcal{R}_w$ should depend on the prior information on each component. For example, for the fibre-crack decomposition problem, the prior for the fibre-component is that it is piecewise constant and its textures mainly follow one direction θ, however, the prior for the crack-component is that it is independent on the direction, piece-wise constant and sparse. Based on these priors we suggest the following regularizations:

$$\mathcal{R}_u(\mathbf{u}) = \lambda_u \mathrm{DTV}_{\theta,a_u}(\mathbf{u}),$$
$$\mathcal{R}_w(\mathbf{w}) = \lambda_w \mathrm{TV}(\mathbf{w}) + \beta\|\mathbf{w}\|_1,$$

where λ_u and λ_w are positive regularization paramters, which control the balance between the fit to the data and the smoothing from the regularizations. With these two regularizations, the both optimization problems in (7) and (8) are convex, and many convex optimization methods can be used to solve them.

4 Image Decomposition Method

In [3, 10], texture-cartoon decomposition methods built on infimal convolution technique are proposed. Based on this work, in this section we introduce another method to decompose directional components from sinogram data.

In many applications fibre-structures are analyzed with the aim to detect cracks and/or other types of deterioration. Whereas the texture of the fibre material follows one main direction θ, the deteriorated parts are mainly perpendicular, or close to perpendicular, to the main direction. Moreover the deteriorated parts are sparse in the object. Based on these observation we propose the following decomposition model:

$$\min_{u\geq 0,w} \frac{1}{2}\|A(\mathbf{u}+\mathbf{w}) - \mathbf{b}\|_2^2 + \lambda\Big(\mathrm{DTV}_{\theta,a_u}(\mathbf{u}) + \alpha\mathrm{DTV}_{\theta^\perp,a_w}(\mathbf{w})\Big) + \beta\|\mathbf{w}\|_{\ell^1}, \tag{9}$$

where $\mathbf{u} \in \mathbb{R}^{M^2}$ represents the fibres, $\mathbf{w} \in \mathbb{R}^{M^2}$ the crack part, and $\lambda, \alpha, \beta > 0$ are regularization parameters. The model (9) is convex, which is desirable when we want to find a solution to the minimization problem. Furthermore the sparsity constraint is not only a reasonable regularization method for $\mathbf{w}$, it also makes (9) strictly convex, i.e. the minimizer will be unique.

We have introduced two different methods for combined decomposition and reconstruction, sinogram splitting method and image decomposition method, and now we sum up the relations and differences between two methods. The sinogram splitting method has a risk to reconstruct incorrect attenuation coefficient values due to split one full scanning problem into two limited angle problems, which are much more complicated for solving. If we use variational methods in (7) and (8) to reconstruct the components, the results are not summable. On the other hand, if we use FBP, based on (6) the components are summable, and

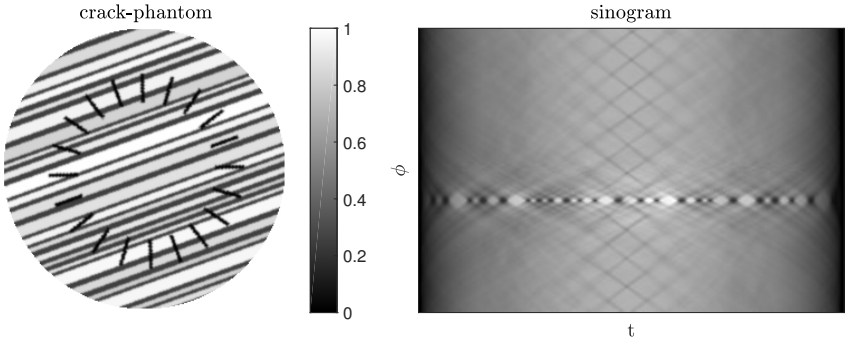

Figure 3: Left: fibre-crack phantom with fibres along the direction 20° and cracks in a circular pattern. Right: simulated noise-free sinogram.

the results are identical to decompose the objects under the constraint (5). In addition, comparing with $\mathcal{R}_u$ and $\mathcal{R}_w$ in (7) and (8), the regularization in (9) plays different role. In (7) and (8) the main purpose of utilizing regularization technique is to remove the limited angle artifacts that occur due to splitting the sinogram, but in (9) the regularization is used for decomposing the components.

5 Numerical Experiments

In this section we demonstrate the performance of the methods introduced in section 3 and 4 two simulated X-ray CT problems. In order to set the stage for the numerical experiments we first give some discretization and experiment details which are valid for the following tests.

We solve the variational optimization problems by using the Primal-Dual-Hybrid-Gradient (PDHG) method proposed in [7] with the stopping rule

$$\frac{|\mathcal{J}(\cdot_{k+1}) - \mathcal{J}(\cdot_k)|}{|\mathcal{J}(\cdot_k)|} < 10^{-5},$$

where $\mathcal{J}$ denotes the objective function. For (9) we solve the subproblems with respect to $\mathbf{u}$ and $\mathbf{w}$ alternately by using PDHG method. All of the algorithms are implemented in Matlab, where we use the parallel beam GPU code described in [18] from the ASTRA toolbox, see [28, 27], to calculate Radon transform and its adjoint operator.

5.1 Sinogram splitting method

For the sinogram splitting method we compare the two reconstruction techniques presented in section 3, namely FBP and the variational method. Both reconstruction methods are tested on a simulated fibre-crack phantom shown in fig. 3, which has cracks in a 360° circular pattern in order to illustrate the performance of decomposition. In the test, the sinogram is simulated with $N_t = 256$ detector bins, $N_\phi = 171$ scanning angles and the reconstruction grid-size is $M = 256$, which make the underdetermined rate as $\frac{N}{M^2} = \frac{2}{3}$. Further, the sinogram is corrupted with 1% additive white Gaussian noise. In Figure 4 we compare the two methods with a split parameter $K = 11$ and centered by the estimated main

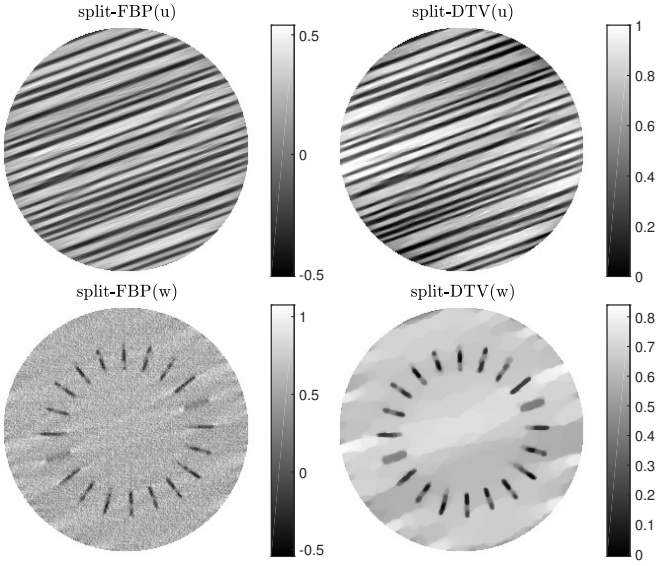

Figure 4: Comparison of two sinogram-splitting methods introduced in section 3.

direction from algorithm 1. For the variational method on splitted sinogram, we choose the optimal λ_u and λ_w based on visual inspection, i.e., the reconstructed $\mathbf{u}$ has clear edges within similar intensity range as the ground truth and $\mathbf{w}$ has a homogeneous background and sharp crack edges.

In Figure 4 we see that both reconstructed fibre components ($\mathbf{u}$) are visually similar, but the colorbar shows that the intensity range by FBP has an offset of arround 0.5. Comparing the reconstructed crack components ($\mathbf{w}$) it is obvious that the result from FBP is much more noisy than the one from the variational method. In addition, all of the cracks are located in the crack components, which is due to a highly directional object and a good choice of the range-width index $K = 10$. An interesting observation is that the cracks along the main direction are also presented in crack components, and the reason is that the boundaries of the crackes which are perpendicular to the main direction are presented in $\mathbf{b}_w$.

To show the role of the parameter K, in Figure 5 we show the results from the variational method with different values of K. It is clear that a small K will result in some fibre elements fallen in the crack-component, whereas a large K will result in some cracks apprearing in the fibre component. The choice of K should be according to prior knowledge about the objects, e.g. if the object is highly directional a relatively low value will be sufficient.

5.2 Image decomposition method

In the image decomposition model (9) several parameters need to be given. The main direction angle θ for fibre component is estimated by algorithm 1, and a_u is fixed as 0.15 based on the empirical tests in [14]. For the crack component, $\theta^{\perp}$ is orthogonal to the main direction, and $a_w = 0.5$ in order to allow to decompose the cracks that are not strictly perpendicular to the main direction and still avoid ending up as TV. In order to avoid one feasible set from the two DTV terms fully covering the other, α should satisfy $a_u < \alpha < \frac{1}{a_w}$, i.e. $0.15 < \alpha < 2$. In the

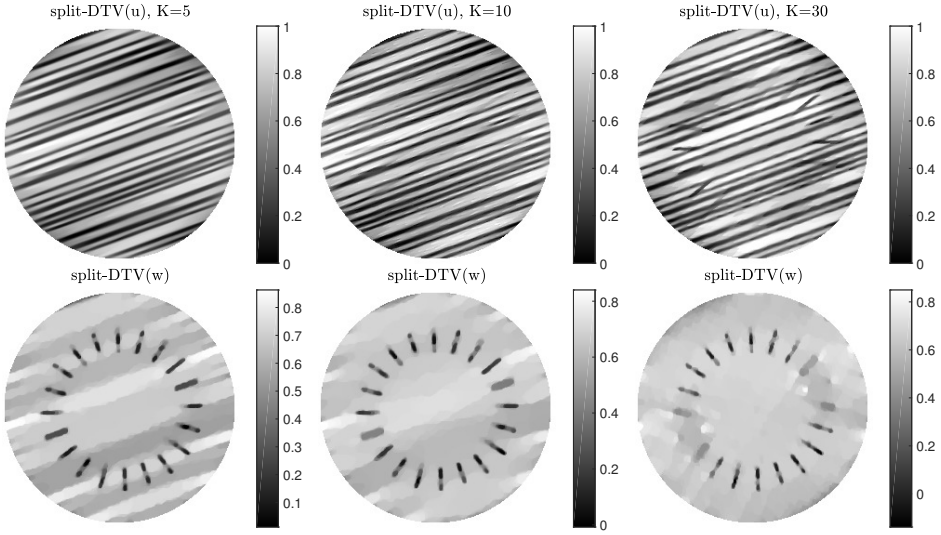

Figure 5: Influence of K on the results from the sinogram splitting method using DTV-regularized reconstruction.

numerical tests, we tune the parameters λ, α and β such that the psnr value of $\mathbf{u} + \mathbf{w}$ to the ground truth $\mathbf{z}$ is maximum.

In Figure 6, we show the reconstruction results with different α values. To avoid that the sparsity constraint influencing the results, we fix $\beta = 10^{-6}$. It is obvious that a small α will result in more details as well as noise in the crack component and a large α will leave many cracks in the fibre component.

In Figure 7, we demonstrate the improvement of including the sparsity constraint in the image decomposition method by comparing the results from $\beta = 10^{-6}$ and $\beta = 10^{-4}$. From the results we see a clear improvement on both components by using larger β. The intensity range for the fibre-component is much more accurate and cracks have much sharper edges. The improvement is also reflected by a slight increase of the psnr value.

5.3 Comparison of the sinogram splitting method with the image decomposition method

Comparing the results shown in Figure 4 and 7, we can see that the sinogram splitting method delivers a much more complete split between the fibres and the cracks along any given direction. From the sinogram splitting method the crack component contains a non-homogeneous background and some artifacts. Furthermore, some cracks are wider than they should be, which is due to the limited scanning angles and the smoothness from the regularization. The image decomposition method performs better on decomposing the cracks along the perpendicular direction to θ because of the regularization. When the sparsity constraint is enforced, we can see that the background of the crack component is homogeneous, while the edges of the cracks are still sharp.

Next, we compare the two methods on a real sample object, which is a carbon fibre sample and shown in Figure 8. The sample is with the size $M = 426$, and

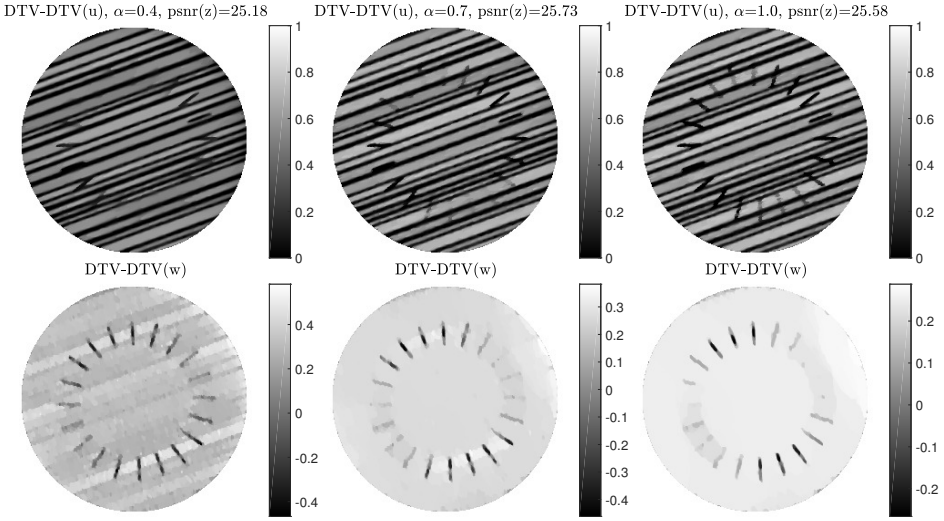

Figure 6: Comparison of the decomposition results from different α by using the image decomposition method.

we simulate $N_t = 426$ detector bins and $N_\phi = 284$ scanning angles with 1% Gaussian noise in the sinogram. In Figure 9 we show the results from FBP-based and variational-based sinogram splitting method as well as image decomposition method. The regularization parameters are tuned based on visual inspection, where we prioritize the decomposition of cracks. In addition, in the sinogram splitting method the range-width index K is set as 120, which is much larger than the one in Figure 4. The reason is to avoid fibre textures appearing in the crack component.

From Figure 9, we can see that the results from the FBP-based sinogram splitting method are clearly influenced by noise and limited angle artifacts. In the results from the variational-based sinogram splitting method the edges of fibres along the main direction are sharp, but other edges are blurry due to the limited scanning angles. In addition, the crack component suffers from a non-homogeneous background and the stair-casing artifacts, which makes it difficult to distinguish cracks. Comparing with the results from the sinogram splitting method, the image decomposition method produces sharper edges in the fibre component and decompose the parts that could be categorized as cracks to the crack component. Especially, the homogeneous background in the crack component will benefit distinguishing cracks.

6 Conclusions

We propose two new tomographic reconstruction methods and aim to decompose components including textures along different directions. We compare the two methods by discussing their theoretical differences, and also propose a new method for estimating the main object direction directly from measured computed tomography data. The proposed methods are compared empirically on both simulated phantom and real object. The simulated phantom tests serves as

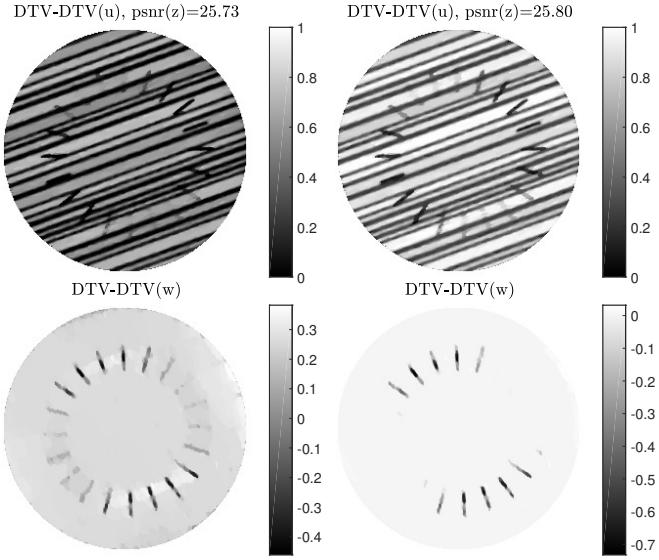

Figure 7: Comparison of the decomposition results from different β by using the image decomposition method. Here, we set $\alpha = 0.7$ and $\lambda = 0.0038$.

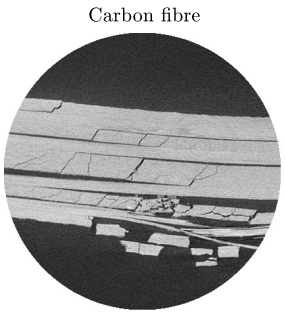

Figure 8: Carbon fibre sample from [21].

a general performance tests of the methods. In these tests we demonstrate what can be achieved with the proposed methods. The real data sample tests show how well these methods perform in practice.

Acknowledgements

The work was supported by Advanced Grant 291405 from the European Research Council.

References

[1] G. Aubert and P. Kornprobst. *Mathematical Problems in Image Processing: Partial Differential Equations and the Calculus of Variations.* Springer Science + Business Media, 2006.

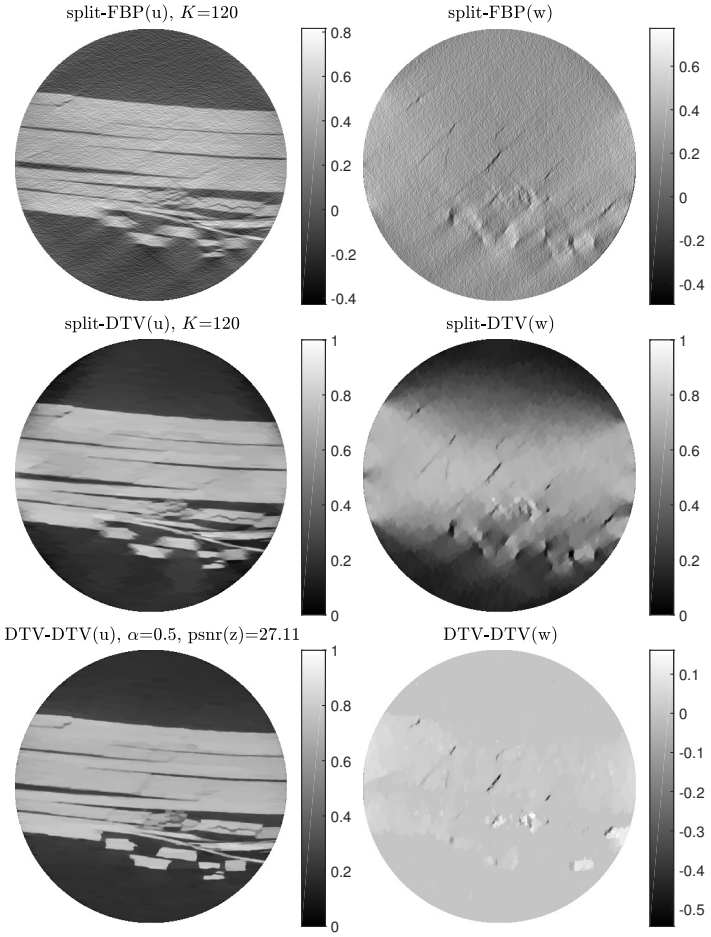

Figure 9: Comparison of the sinogram splitting method with the image decomposition method on real objects.

[2] J. F. Aujol, G. Aubert, L. Blanc-Féraud, and A. Chambolle. Image decomposition into a bounded variation component and an oscillating component. *J. Math. Imaging Vis.*, 22(1):71–88, 2005.

[3] J. F. Aujol, G. Gilboa, T. Chan, and S. Osher. Structure-texture image decomposition-modeling, algorithms, and parameter selection. *Int. J. Comput. Vis.*, 67(1):111–136, 2006.

[4] I. Bayram and M. E. Kamasak. A directional total variation. *Eur. Signal Process. Conf.*, 19(12):265–269, 2012.

[5] T. M. Buzug. *Computed Tomography : From Photon Statistics to Modern Cone-Beam CT*. Springer, 2008.

[6] A. Chambolle and P.-L. Lions. Image recovery via total variation minimization and related problems. *Numer. Math.*, 76(2):167–188, 1997.

[7] A. Chambolle and T. Pock. A first-order primal-dual algorithm for convex problems with applications to imaging. *J. Math. Imaging Vis.*, 40(1):120–145, dec 2011.

[8] A. H. Delaney and Y. Bresler. Globally convergent edge-preserving regularized reconstruction: An application to limited-angle tomography. *IEEE Trans. Image Process.*, 7(2):204–221, 1998.

[9] S. Esedoglu and S. J. Osher. Decomposition of images by the anisotropic Rudin-Osher-Fatemi model. *Commun. Pure Appl. Math.*, 57(12):1609–1626, 2004.

[10] J. Gilles. Noisy image decomposition: A new structure, texture and noise model based on local adaptivity. *J. Math. Imaging Vis.*, 28(3):285–295, 2007.

[11] M. Holler and K. Kunisch. On infimal convolution of total tariation type functionals and applications. *SIAM J. Imaging Sci. J. Imaging Sci.*, 7(4):2258–2300, 2014.

[12] K. M. Jespersen, J. Zangenberg, T. Lowe, P. J. Withers, and L. P. Mikkelsen. Fatigue damage assessment of uni-directional non-crimp fabric reinforced polyester composite using X-ray computed tomography. *Compos. Sci. Technol.*, 136:94–103, 2016.

[13] R. D. Kongskov and Y. Dong. Directional total generalized variation regularization for impulse noise removal Rasmus. *Scale Sp. Var. Methods Comput. Vis. 2017*, 6667:221–231, 2017.

[14] R. D. Kongskov, Y. Dong, and K. Knudsen. Directional total generalized variation regularization. *http://arxiv.org/abs/1701.02675*, 2017.

[15] V. P. Krishnan and E. T. Quinto. *Handbook of Mathematical Methods in Imaging*. Springer Science + Business Media, 2015.

[16] J. Li, C. Miao, Z. Shen, G. Wang, and H. Yu. Robust frame based x-ray ct reconstruction. *Journal of Computational Mathematics*, 34(6):683, 2016.

[17] Y. Meyer. *Oscillating Patterns in Image Processing and Nonlinear Evolution Equations*, volume 22. American Mathematical Society, 2001.

[18] W. J. Palenstijn, K. J. Batenburg, and J. Sijbers. Performance improvements for iterative electron tomography reconstruction using graphics processing units (GPUs). *J. Struct. Biol.*, 176(2):250–253, 2011.

[19] E. T. Quinto. Singularities of the X-ray transform and limited data tomography in $\mathbb{R}^2$ and $\mathbb{R}^3$. *SIAM J. Math. Anal.*, 24(5):1215–1225, 1993.

[20] J. Radon. Über die Bestimmung von Funktionen durch ihre Integralwerte längs gewisser Mannigfaltigkeiten. *Akad. Wiss.*, 69:262–277, 1917.

[21] J. E. Rouse. *Characterisation of Impact Damage in Carbon Fibre Reinforced Plastics by 3D X-Ray Tomography*. PhD thesis, University of Manchester, 2012.

[22] L. I. Rudin, S. Osher, and E. Fatemi. Nonlinear total variation based noise removal algorithms. *Phys. D Nonlinear Phenom.*, 60(1-4):259–268, 1992.

[23] S. R. Sandoghchi, G. T. Jasion, N. V. Wheeler, S. Jain, Z. Lian, J. P. Wooler, R. P. Boardman, N. K. Baddela, Y. Chen, J. R. Hayes, E. N. Fokoua, T. Bradley, D. R. Gray, S. M. Mousavi, M. N. Petrovich, F. Poletti, and D. J. Richardson. X-ray tomography for structural analysis of microstructured and multimaterial optical fibers and preforms. *Opt. Express*, 22(21):26181, 2014.

[24] O. Scherzer. *Handbook of Mathematical Methods in Imaging*. Springer Science + Business Media, 2010.

[25] E. Y. Sidky and X. Pan. Image reconstruction in circular cone-beam computed tomography by constrained, total-variation minimization. *Phys. Med. Biol.*, 53(17):4777–4807, sep 2008.

[26] J. L. Starck, M. Elad, and D. L. Donoho. Image Decomposition via the combination of sparse representation and a variational approach. *IEEE Trans.Image Process.*, 14(10):1570–1582, 2005.

[27] W. van Aarle, W. J. Palenstijn, J. Cant, E. Janssens, F. Bleichrodt, A. Dabravolski, J. De Beenhouwer, K. Joost Batenburg, and J. Sijbers. Fast and flexible X-ray tomography using the ASTRA toolbox. *Opt. Express*, 24(22):25129, 2016.

[28] W. van Aarle, W. J. Palenstijn, J. De Beenhouwer, T. Altantzis, S. Bals, K. J. Batenburg, and J. Sijbers. The ASTRA Toolbox: A platform for advanced algorithm development in electron tomography. *Ultramicroscopy*, 157:35–47, 2015.